JACS
JOURNAL OF THE AMERICAN CHEMICAL SOCIETY

Article

Polar solvent induced lattice distortion of cubic CsPbI3 nanocubes and hierarchical self-assembly into orthorhombic single-crystalline nanowires

Jian-Kun Sun, Sheng Huang, Xiao-Zhi Liu, Quan Xu, Qing-Hua Zhang, Wen-Jie Jiang, Ding-Jiang Xue, Jia-Chao Xu, Jing-Yuan Ma, Jie Ding, Qian-Qing Ge, Lin Gu, Xiaohong Fang, Hai-Zheng Zhong, Jin-Song Hu, and Li-Jun Wan

J. Am. Chem. Soc., **Just Accepted Manuscript** • DOI: 10.1021/jacs.8b05949 • Publication Date (Web): 15 Aug 2018

Polar Solvent Induced Lattice Distortion of Cubic $CsPbI_3$ Nanocubes and Hierarchical Self-assembly into Orthorhombic Single-crystalline Nanowires

Jian-Kun Sun,[†,§,▽] Sheng Huang[‡,▽], Xiao-Zhi Liu,[//] Quan Xu,[†,§] Qing-Hua Zhang,[//] Wen-Jie Jiang,[†,§] Ding-Jiang Xue,[†,§] Jia-Chao Xu,[†,§] Jing-Yuan Ma,[†,§] Jie Ding,[†,§] Qian-Qing Ge,[†,§] Lin Gu,[//] Xiao-Hong Fang,[†,§] Hai-Zheng Zhong,[‡] Jin-Song Hu,*[,†,§] Li-Jun Wan*[,†,§]

[†] CAS Key Laboratory of Molecular Nanostructure and Nanotechnology, Beijing National Research Center for Molecular Sciences, CAS Research/Education Center for Excellence in Molecule Science, Institute of Chemistry, Chinese Academy of Sciences, Beijing 100190, China.

[‡] Beijing Key Laboratory of Nanophotonics asnd Ultrafine Optoelectronic Systems, School of Materials Science & Engineering, Beijing Institute of Technology, Zhongguancun South Street, Haidian District Beijing, 100081, China.

[//] Beijing National Laboratory for Condensed Matter Physics, Collaborative Innovation Center of Quantum Matter, Institute of Physics, Chinese Academy of Sciences, Beijing 100190, China

[§] School of Chemical Sciences, University of Chinese Academy of Sciences, Beijing 100049, China

KEYWORDS: Perovskites, Polar solvent, $CsPbI_3$, Lattice distortion, Self-assembly, Phase transition

ABSTRACT: Despite the recent surge of interest in inorganic lead halide perovskite nanocrystals, there are still significant gaps in their stability disturbance and the understanding of their destabilization, assembly, and growth processes. Here, we discover that polar solvent molecules can induce the lattice distortion of ligand-stabilized cubic $CsPbI_3$, leading to the phase transition into orthorhombic phase which is unfavorable for photovoltaic applications. Such lattice distortion triggers the dipole moment on $CsPbI_3$ nanocubes, which subsequently initiates the hierarchical self-assembly of $CsPbI_3$ nanocubes into single-crystalline nanowires. The systematic investigations and in-situ monitoring on the kinetics of the self-assembly process disclose that the more amount or the stronger polarity of solvent can induce the more rapid self-assembly and phase transition. These results not only elucidate the destabilization mechanism of cubic $CsPbI_3$ nanocrystals, but also open up opportunities to synthesize and store cubic $CsPbI_3$ for their practical applications in photovoltaics and optoelectronics.

1. Introduction

Hybrid organic-inorganic halide perovskites have emerged as intriguing photovoltaic materials and achieved a certified power conversion efficiency (PCE) of > 22 %, on a par with the best single-junction chalcogenide and silicon devices.[1] However, the intrinsic structural instability leads to their dissociation into PbX_2 and volatile organic halide under environmental moisture or heat, technically hurdling the commercialization at the current stage.[2-4] Instead, all-inorganic lead halide perovskites are explored to tackle this issue by replacing volatile organic components. $CsPbX_3$ are promising candidates since Cs^+ is the most feasible inorganic cation to occupy ammonium sites with suitable tolerance factor.[5-7] Although cubic $CsPbBr_3$ is relatively stable and shows great potential as light-emitting semiconductor,[8-13] the too wide bandgap (E_g = 2.25 eV) makes it not suitable for single-junction photovoltaics.[14,15] Cubic (α) $CsPbI_3$ has the most appropriate bandgap of 1.7 eV for high-efficiency photovoltaics, but not thermodynamically preferred. It will transit spontaneously into the room-temperature stable yellow δ-phase (orthorhombic non-perovskite double chain phase) with an improper bandgap (Eg = 3.0 eV) over time. Although the yellow non-perovskite δ-phase can be converted to the black perovskite α-phase upon heating above 360 °C, it will convert sequentially to the black β-phase and γ-phase with slightly distorted perovskite structure up cooling, and eventually convert back to thermodynamically preferred non-perovskite yellow δ-phase.[16]

A couple of strategies have been explored to alleviate this phase-change issue.[17-25] Alloying with Br^- is able to significantly reduce the phase-transition temperature down to ~110 °C although at a cost of increasing bandgap.[18,19,26] Protesescu et al. reported that $CsPbI_3$ nanocrystals with oleic acid and oleylamine as ligands could keep cubic phase at room temperature.[20] Luther etc. demonstrated that the surface energy-leveraged cubic $CsPbI_3$ quantum dots (QDs) could achieve over 10 % of PCE on a PV device.[21] The surface modification with ethylenediamine cation (EDA^+), formamidinium (FA^+), or methylammonium (MA^+) were subsequently reported by Zhao and Luther etc. to stabilize cubic phase, pushing the cell PCE up to 13.43 %.[22,23] Several examples also demonstrated that the organic surface ligands played an important role in controlling the size and shape of $CsPbX_3$ nanocrystals[27-30]. $CsPbX_3$ nanocubes, nanodots, nanoplates, nanorods, stacked column etc. were synthesized by mediating organic ligands although the underline mechanism still needs to be unveiled and phase control is still challenging.[31-33] Therefore, understanding the role of surface ligands on the structural evolution of $CsPbI_3$ is essential to explore the ambient-stable $CsPbI_3$ for photovoltaic and light-

emitting applications.

Herein, we report for the first time that polar solvent molecules can induce the lattice distortion of ligand-stabilized cubic $CsPbI_3$, triggering the dipole moment which subsequently initiates the hierarchical self-assembly of $CsPbI_3$ nanocubes into single-crystalline nanowires via oriented attachment (OA) process. Theoretical analyses indicate that the adsorption of polar molecule such as ethanol causes the move of metal cation and the distortion of PbI_6 octahedrons in cubic $CsPbI_3$, which is directly proved by atomic-resolution transmission electron microscopic observation. Such lattice distortion initiates the dipole moment on $CsPbI_3$ nanocubes where it should not intrinsically exist if the symmetry is not broken. Driven by the dipole-dipole force, the distorted nanocubes self-assemble and re-crystallize into single-crystalline nanowire in a same width as the size of a nanocube under OA mechanism, accompanying with the phase transition from cubic into orthorhombic phase. These nanowires can further self-assemble side-by-side into thick single-crystalline nanowire with a diameter up to submicron to minimize the surface energy. Unlike the OA growth in inorganic semiconductor nanocrystal systems (such as CdS, CdTe and PbSe etc.), the OA self-assembly of $CsPbI_3$ nanocubes into nanowires/microwires is significantly accelerated due to the easy migration of cations in halide perovskites.[34-37] These findings not only shed light on the phase transition of organic ligands-stabilized cubic inorganic halide perovskites in polar solvents, guiding the exploration of room-temperature stable cubic $CsPbI_3$ for optoelectronic applications, but also reveal how the perovskite nanocubes in a size of ~10 nm evolve into single-crystalline nanowires in a length of several micrometers and a diameter up to submicron.

2. Experimental Section

2.1 Chemicals and Materials. Cesium carbonate (Cs_2CO_3, 99.99 %), lead(II) iodide (PbI_2, 99.999 %), 1-octadecene (ODE, 90 %), oleic acid (OA, 90 %), and oleylamine (OAm, 90 %) were purchased from Sigma-Aldrich. All these chemicals were used as received without any further purification. Methanol (Innochem, 99.9%), ethanol (Acros, 99.8 %), acetone (Acros, 99.9 %), isopropanol (Alfa, 99.9 %), methyl acetate (Acros, 99+%), and n-hexane (Innochem, 97.5%) were used for investigating the influence of solvent polarity on the stability of $CsPbI_3$ nanocrystals. All these solvents were dried with molecular sieves and stored in glove box prior to use.

2.2 Synthesis of $CsPbI_3$ nanocubes. $CsPbI_3$ nanocubes were synthesized according to modified previous procedures.[20] In brief, Cs-oleate precursors were firstly prepared as follows. 0.0814 g Cs_2CO_3, 0.5 mL OA, and 10 mL ODE were loaded in a 50 mL 3-neck flask and degassed at 120 °C for 1 h under vacuum, then heated up to 150 °C under N_2 flow until all Cs_2CO_3 were reacted with OA. The Cs-oleate precursor solution was kept at 100 °C to prevent its precipitation out of ODE. In another 50 mL 3-neck flask, 0.1734 g PbI_2 and 10 mL ODE were degassed under vacuum at 120°C for 1 h. Afterwards, 1 mL dried OAm and 1 mL OA were injected into the flask under N_2 flow. After PbI_2 completely dissolved, the reaction temperature was raised to 170 °C and 0.8 mL Cs-oleate was swiftly injected. 5 s later, the suspension was cooled down by ice-water bath, then centrifugalized to collect the solid products. The products were then redispersed into hexane and centrifuged again. The supernatant was filtered and store in glove box for further use in the following experiments.

2.3 Self-assembly of $CsPbI_3$ nanocubes. The self-assembly and phase transition were induced by introducing polar solvents. In a typical procedure, 2 mL of $CsPbI_3$ nanocrystal dispersion in hexane containing ~2 mmol CsPbI3 were dispensed into glass vials which cap has an injectable rubber in the middle. The polar solvent mixing was carried out by injecting 0.1 mL solvent taken from glove box under a constant stirring of 600 RPM via a syringe pump at an rate of 0.5 mL/min.

2.4 Characterizations. Fourier transform infrared spectroscopy (FTIR) spectra were measured on TENSOR-27 (Bruker). Transmission electron microscopy (TEM) images were recorded using a JEOL JEM-2100F microscopy, working at an accelerating voltage of 200 kV. The high-angle annular dark-field (HAADF) imaging experiments were performed on an ARM-200F (JEOL, Tokyo, Japan) STEM operated at 200 kV with a CEOS Cs corrector (CEOS GmbH, Heidelberg, Germany). It should be noted that the TEM sample should be prepared and transferred as quickly as possible in dry condition since the exposure to moisture will cause the change of cubic nanocrystals over time in view of high polarity of water. Powder X-ray diffraction (XRD) patterns were recorded on a Rigaku D/Max-2500 diffractometer equipped with a Cu Kα1 radiation ($\lambda =$ 1.54056 Å) at a scan rate of 3° min^{-1}. A home-built total internal reflection fluorescence microscope (TIRFM) with a resolution of single-molecule imaging was used to monitor the fluorescence during the self-assembly. The UV-vis absorption spectra were collected on a UV-vis spectrophotometer (UH4150, HITACHI). Photoluminescence (PL) spectra were measured in an Edinburgh Instrument FLS 980 spectrophotometer.

2.5 Surface energy calculations. We use the equation (1) to calculate the surface free energy γ_{abc} of a (abc) crystal face.

$$\gamma = \frac{\Delta E}{\Delta A} \quad (1)$$

where ΔE represents the free energy difference between the material with new surface, and ΔA is the area of the surface. For a slab the surface energy can be determined as,[38-40]

$$\gamma = \frac{(E_{slab}^{N} - NE_{bulk})}{2A} \quad (2)$$

where N is the number of layers in the slab, E_{slab}^{N} is the total energy of an N-layer slab, E_{bulk} represents the energy of a formula unit of bulk material, which can be treated as a monolayer. A is the area of the surface. The calculation is based on the density functional theory (DFT), which is performed by the PWmat code. A DFT Plane Wave materials

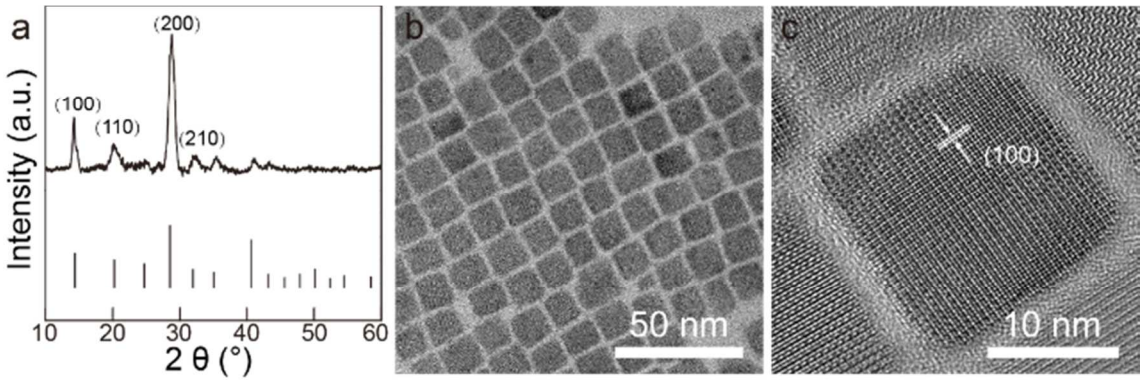

Figure 1. Pristine $CsPbI_3$ nanocubes. (a) XRD patterns. (b-c) TEM images at low- (b) and high- (c) magnification.

simulation code run on GPU clusters. The pseudo potential adopted the USPP-GBRV.[41,42] In all models, we set the value of the vacuum regions is 10 □ and N equal to 5. K point grids of 2×2×2 are chosen for all systems. The structural parameters of orthorhombic non-perovskite $CsPbI_3$ are based on the reference (JCPDS No. 74-1970), i.e., a = 4.797 Å, b = 10.462 Å, c = 17.788 Å, and α = β = γ =90°.

2.5 Adsorption energy calculations.

The adsorption energy is calculated according to the following equation 3,

$$E_{adsorb} = E_{complex} - E_{ligand} - E_{CsPbI_3} \quad (3)$$

Where $E_{complex}$, E_{ligand}, E_{CsPbI_3} are the total energies of the adsorbed complex, ligand and $CsPbI_3$ perovskites, respectively.

2.6 Dipole moment calculations. The dipole moment of single relaxed primitive unit cell is carried out by Gaussian09 code.[43] We use the HF/Lanl2dz as the basis sets. The value of the dipole moment is 3.5 Debye.

We compute the distribution of dipolar potential field with the following formula,[44]

$$\hat{H} = \sum_{dipole,dipole}^{n,m} \frac{1}{4\pi\varepsilon_0\varepsilon_r}\left(\frac{p_i p_j}{r^3} - \frac{3(\hat{n}p_i)(\hat{n}p_j)}{r^3}\right) \quad (4)$$

where p_i represents the dipole moment; $\hat{n}$ is the unit vector along the vector r between the dipoles; ε_0 is the dielectric constant of vacuum; and ε_r is the relative dielectric constant.

3. Results and Discussion

3.1 Characterization of CsPbI3 nanocubes. $CsPbI_3$ nanocubes were first characterized by XRD technique. All XRD peaks in Figure 1a matches with those simulated from single-crystalline cubic $CsPbI_3$ (ICSD #161481), indicating that the product is cubic $CsPbI_3$. Transmission electron microscope (TEM) image (Figure 1b) shows that the product is composed of uniform and nearly perfect nanocubes in a size of around 14 ± 2 nm. High-resolution TEM image in Figure 1c clearly displays the lattice fringes with a distance of 0.63 nm from the (100) planes of cubic $CsPbI_3$. It is known that bulk $CsPbI_3$ tends to crystallize in orthorhombic phase at room temperature. The cubic phase of $CsPbI_3$ nanocubes here can be attributed to the stabilization of surface ligands.[28,45] It is reported that oleylamine ions (OAMIs) can attach to $CsPbI_3$ nanocrystals via electrostatic interactions with surface iodide ions and oleic acid can interacts with the ammonium head group of OAMIs to form a bilayer-type protection ligand layer.[46] FTIR spectrum confirms the existence of oleic acid and alkylammonium cations as surface ligands on these nanocubes (Figure S1). As shown in Figure 1b and c, $CsPbI_3$ nanocubes are distributed equidistantly, which is the result of multiple interactions. In general, the interactions between two charged nanocrystals include steric and osmotic repulsion, van der Waals attraction, and electrostatic interaction (such as charge-charge, charge-dipole, dipole-dipole, charge-induced dipole interactions).[47-49] Since the dipole moment of a highly symmetric nanocube is nearly zero, the electrostatic interaction is charge-charge interaction. Therefore, the $CsPbI_3$ nanocubes in equilibrium are under steric repulsion (supported by ligand chains), van der Waals attraction, and charge-charge interaction. The distance among $CsPbI_3$ nanocubes of ~2 nm (Figure 1c) is the thickness of interdigitated capping ligands.[47]

3.2 Polar solvent induced lattice distortion of $CsPbI_3$ nanocubes. As discussed above, the as-synthesized $CsPbI_3$ nanocubes can be stabilized in cubic phase by OAMIs and oleic acid.[20] However, these ligands are not favorable for carrier transportation and need to be removed before the fabrication of optoelectronic devices.[50] In our experiments, we found that the polarity of washing solvent significantly influenced the stability of $CsPbI_3$ nanocubes. The polar molecules could induce the lattice distortion and phase transition of cubic $CsPbI_3$. To get clear insight into the influence of polar solvent on the lattice distortion, we use aberration corrected scanning transmission electron microscope (AC-STEM) to reveal the structural evolution in atomic resolution before and after the introduction of ethanol (an example of polar molecules). Without ethanol, high angle annular dark-field (HAADF) STEM image of a pristine $CsPbI_3$ nanocube (Figure 2a) clearly shows the atomic structure of cubic-phase perovskite. Figure 2b and Figure 2c are the zoom-in view of the inner and outer parts marked by red and yellow squares in Figure 2a, respectively. Pb-I columns, Cs atom column, and I column are labeled as red, cyan and purple dots, respectively. It is obvious that

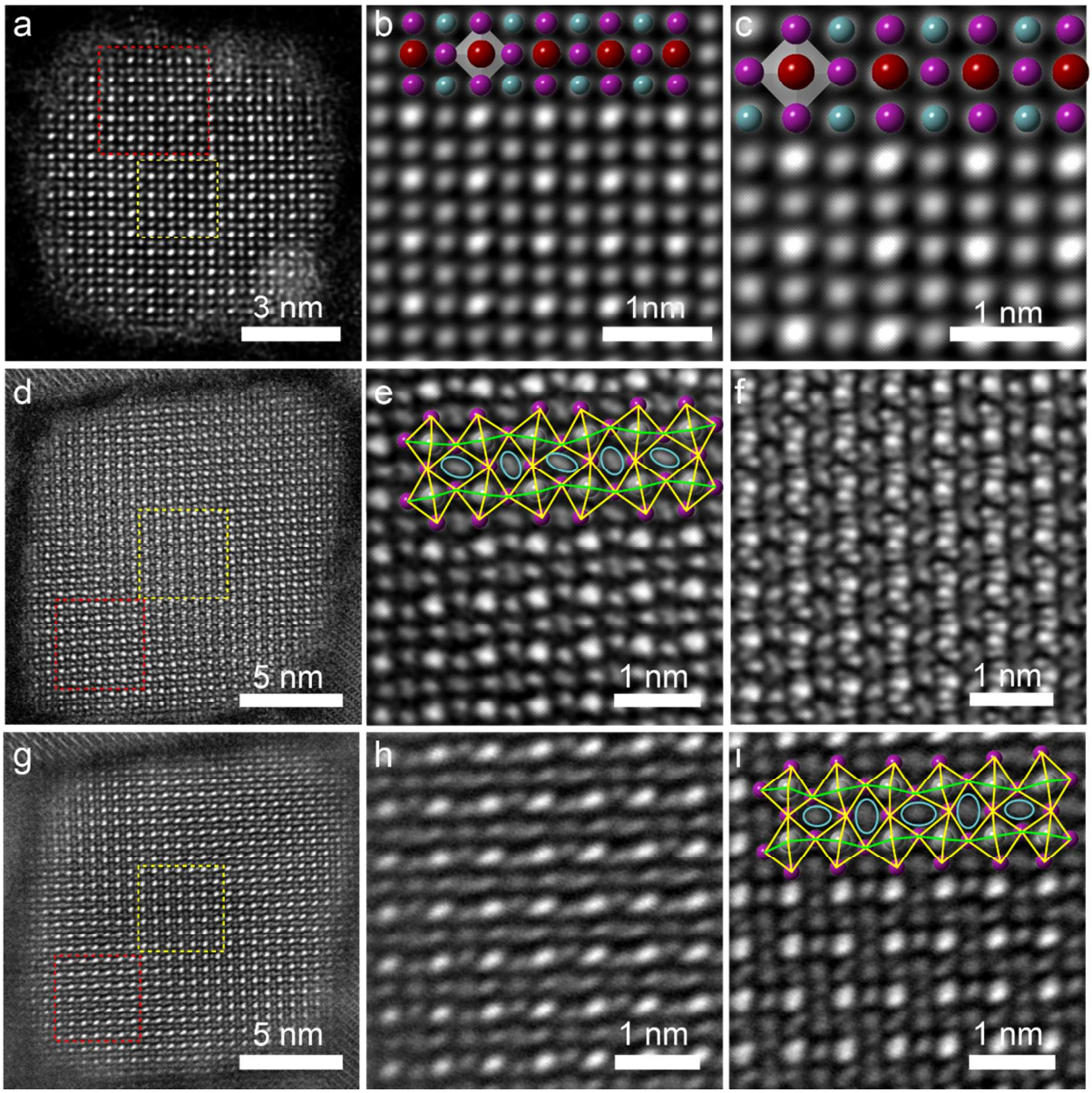

Figure 2. HAADF images of the pristine and ethanol-adsorbed $CsPbI_3$ nanocrystal. (a) HAADF image of the pristine $CsPbI_3$ nanocrystal. (b-c) Zoom-in view of the outer and the inner area in (a), marked with a red and yellow square, respectively. Red, cyan and purple dots, represent Pb-I column, Cs atoms and I atoms column. Pb-I_6 octahedra along [001] projection are overlaid on the image. (d-i) HADDF images of ethanol-adsorbed $CsPbI_3$ (et-$CsPbI_3$) nanocrystal. (d) HADDF images with zone axis perpendicular to the outer planes of et-$CsPbI_3$. (e-f) Zoom-in image corresponding to the outer red square and center yellow square in (d). (g) HADDF images with zone axis perpendicular to the center planes of et-$CsPbI_3$. (h-i) Zoom-in image of the outer and the inner area of et-$CsPbI_3$ in red and yellow square in (g).

both inner and outer parts of $CsPbI_3$ nanocube exhibit the perfect distortion-free cubic perovskite structure in the [001] projection where Pb-I column is in a higher contrast compared with Cs atoms or I atoms column. No structural distortion is observed on the whole nanocube. While HAADF STEM images (Figure 2d-i) displays the clear lattice distortion after introducing ethanol into the dispersion of as-synthesized $CsPbI_3$ nanocubes. By aligning the incident electron beam to the zone axis of the outer nanocube, the zoom-in view (Figure 2e) of red-square area in Figure 2d clearly shows that the Pb-I-Pb configuration deviates from its original linear states (as shown in Figure 2b), resulting in a "zig-zag" structure. Concomitantly, the overlapped Cs atom column projected along [001] direction evolves from dot shape into oval shape, as marked by blue ellipses, indicating the movement of Cs column in octahedral cavities. Moreover, the inner part of $CsPbI_3$ nanocube (yellow-square area) displays complex pattern due to the misalignment between the electron beam and the zone axis of the inner nanocube (Figure 2f),

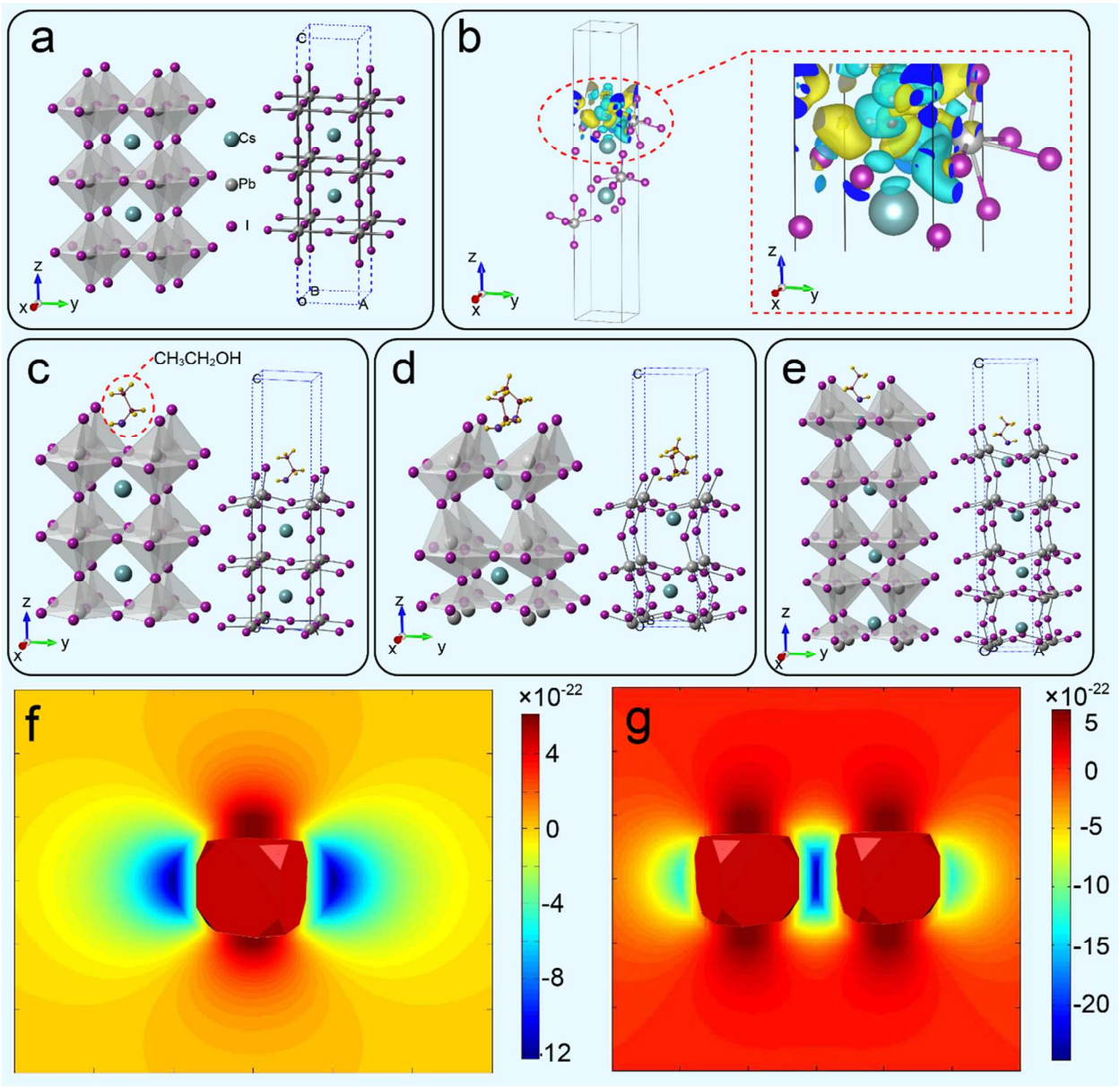

Figure 3. (a-e) Polyhedral and ball-and-stick model of $CsPbI_3$. Aquamarine blue, gray and purple spheres represent Cs, Pb, I atoms, respectively. (a) Cubic $CsPbI_3$. (b) Differential charge density of ethanol molecule adsorbed $CsPbI_3$ (cyan represents the area of losing electrons, while yellow is gaining electron. Blue is the cross profile). (c-e) Results of ethanol molecules adsorbed on $CsPbI_3$ structure with different layers. (f-g) Distribution of dipolar potential field around one or two adjacent $CsPbI_3$ nanoparticles induced by ethanol molecules.

corroborating the apparent distortion generated from outside and penetrated to inside of nanocube. By aligning the incident electron beam to the zone axis of the inner nanocube, the similar distorted cubic pattern could be obtained as shown in Figure 2g. As the distortion directions of adjacent atom columns are apparently distinct from each other, the Pb-I-Pb "zig-zag" configuration can be seen in both Figure 2h and 2i, confirming the lattice distortion occurs in the whole nanocube in the presence of ethanol molecules. These results reveal at atomic scale that the ethanol molecules can induce the rotation and distortion of the corner-sharing PbI_6 octahedrons and offset of Cs atoms in octahedrons cavities throughout whole $CsPbI_3$ nanocube.

3.3 Theoretic analysis of polar solvent induced lattice distortion. DFT calculations were carried out to get further insight into the polar molecule induced lattice distortion of cubic $CsPbI_3$. As shown in Figure 3a, cubic $CsPbI_3$ belongs to a space group $Pm\bar{3}m$ with high symmetry. I atoms occupy the vertices of regular corner-sharing PbI_6 octahedra, while divalent Pb atoms sit at the octahedra centers. The monovalent Cs atoms are hosted by a cavity enclosed by neighboring octahedra. We first simulated the adsorption process of ethanol molecule on $CsPbI_3$ with alkylamine surface ligands. Results show that ethanol molecule prefers to impact onto $CsPbI_3$ instead of attacking alkylamine ligand. As shown in Figure S2, the adsorption of ethanol on $CsPbI_3$ crystal is spontaneous and the attachment of ethanol molecule will release energy. In contrast, breaking iodide ion and alkylamine

ligand is an endothermic process. Therefore, when ethanol molecules approach$CsPbI_3$ nanocubes, they prefer to attach onto $CsPbI_3$ rather than attack surface ligands. Based on this result and considering the computation consume, we use two-layer cubic $CsPbI_3$ structural units without surface ligands for further modelling the impact of ethanol molecules. The differential charge density profile (Figure 3b) of ethanol-adsorbed $CsPbI_3$ (where cyan represents the area of losing electrons and yellow is gaining electron) corroborates Cs atoms in cubic structure are independently filled in the cavity without polarity, while polar molecule can induce the shift of electron cloud of Cs and thus polarity. From Figure 3b, it can be seen that Cs^+ loses electron when the ethanol molecules are adsorbed on $CsPbI_3$, resulting in symmetry breaking of PbI_6 octahedra nearby and the polarization of $CsPbI_3$. This result agrees with the energy calculation. The mulliken charge data (Table S1) gives the specific charge value of original cubic and polarized $CsPbI_3$. The increased charge values of Cs atoms justify the increased electropositivity and electron loss, verifying the polarization effect of ethanol molecule on cubic $CsPbI_3$. This means that the adsorption of ethanol molecule leads to the migration of Cs cation, following by distortion of PbI_6 octahedra and octahedral cavities (Figure 3c-e) in view of the shifting in Pb-I lengths and Pb-I-Pb angles. As listed in Table S2, when one ethanol molecule absorbed on a two-layer cubic $CsPbI_3$ unit, Pb-I bond length on the first and second layer deviate from its original length of 3.174 Å by 0.0897 Å and 0.0580 Å, respectively; and Pb-I-Pb bond angle deviates by 6.5340° from its original value of 180°. Further calculation was carried out by using two ethanol molecules. As shown in Figure 3c-d, the movement of metal cations and the distortion of PbI_6 octahedrons are intensified compared with the one-molecule case. Specifically, When two ethanol molecule attacks, Pb-I bond length on the first and second layer shifts 0.1228 Å and 0.1384 Å, respectively; and Pb-I-Pb bond angle shifts by 14.5560° (Table S2). These results indicates that more ethanol molecules will aggravate the polarization deformation of $CsPbI_3$. Moreover, even if expanding the $CsPbI_3$ models, the movement and distortion can be observed throughout the whole model, as shown in Figure 3e. To further understand the adsorption process of polar molecules, we simulate the adsorption of ethanol molecules from different sides (Figure S3). Calculated results indicate that the attachment energy for ethanol molecules from opposite side (ΔQ_1 = -1.7235 eV) is just slighter lower than that for ipsilateral adsorption (ΔQ_2 = -1.9819 eV) and the lattice distortion occurs in both cases. This result suggests that the ethanol molecules can adsorb on $CsPbI_3$ crystals from either ipsilateral side or opposite sides, inducing the lattice distortion of cubic $CsPbI_3$ to non-symmetric configuration.

Although cubic $CsPbI_3$ nanocube is a highly symmetric structure with no dipole moment in original state, the dipole moment can be created after the lattice distortion induced by ethanol molecules via breaking the symmetry. Figure 3f-g simulate the distribution of the dipolar potential field of one or two $CsPbI_3$ nanocubes at the existence of ethanol molecules, respectively. In the dipolar potential field of two-polarized $CsPbI_3$ nanoparticles, when another similarly polarized-$CsPbI_3$ nanocrystal approached, the gradient of the dipole filed would be the smallest along the rectilinear direction from the side of the opposite charged end of the dipole; and the energy state of the approached nanoparticle is the lowest and most stable. This explains that the polarized-$CsPbI_3$ nanoparticles tends to arrange in a line.

3.4 Polar solvent induced hierarchal self-assembly of $CsPbI_3$ nanocubes. As mentioned above, although the cubic $CsPbI_3$ nanocube itself does not show dipole moment, the attachment of polar molecules induces its lattice distortion, generating the dipole moment which can initiate the self-assembly of these nanocubes. After the introduction of ethanol, the structure deformation and crystal polarization cause the decrease of surface energy and the fall-off of alkylamine ligands, leading to the decline of steric repulsion among $CsPbI_3$ nanocubes. Meanwhile, the dipole-dipole attraction, i.e., orientation force, will attract them closer. As evidenced in Figure 4a-d and Figure S4, the inter-distances of nanocubes clearly shrink over time. For example, the statistic results on a basis of TEM observations show that the inter-distance decreases from 1.92 nm at initial stage to 1.36, 1.07, then 0.76 nm after 1, 2.5, and 5 min since the addition of ethanol, respectively (Figure S4). Due to the lowest field gradient and energy distribution in the aligning direction of nanocubes (Figure 3g), the polarized $CsPbI_3$ nanocubes tends to align in a line under multiple interactions (Figure 4c, d). At the same time, the ethanol-induced polarization of $CsPbI_3$ nanocube increases over time, resulting in its further distortion and peel-off of amine ligands. Once the nanocubes get attached, they fuse together into a single-crystalline elongated nanocrystals to reduce the surface energy (Figure 4e, f), like what happens in the oriented attachment growth of nanocrystals.[51] Since the cubic-phase $CsPbI_3$ is thermodynamically unstable at room temperature, the nanocubes were stabilized by the surface energy of organic amine ligands. Accompanying with ligand peel-off and lattice fusion, the cubic $CsPbI_3$ nanocrystals undergo the phase transformation into thermodynamically stable orthorhombic phase, which has a lower internal energy than cubic phase as calculated in Figure S5. The lattice fringes and corresponding Fourier-transformed diffractograms in HRTEM image (Figure 4f) confirms that the fused nanocrystal is becoming orthorhombic structure (red square region), while the approaching nanocube still remains in distorted cubic phase (white square region).

Concomitant with such nanocrystal fusion, the anisotropic interactions, such as the electric dipole force, will be enhanced in the aligning direction, further driving

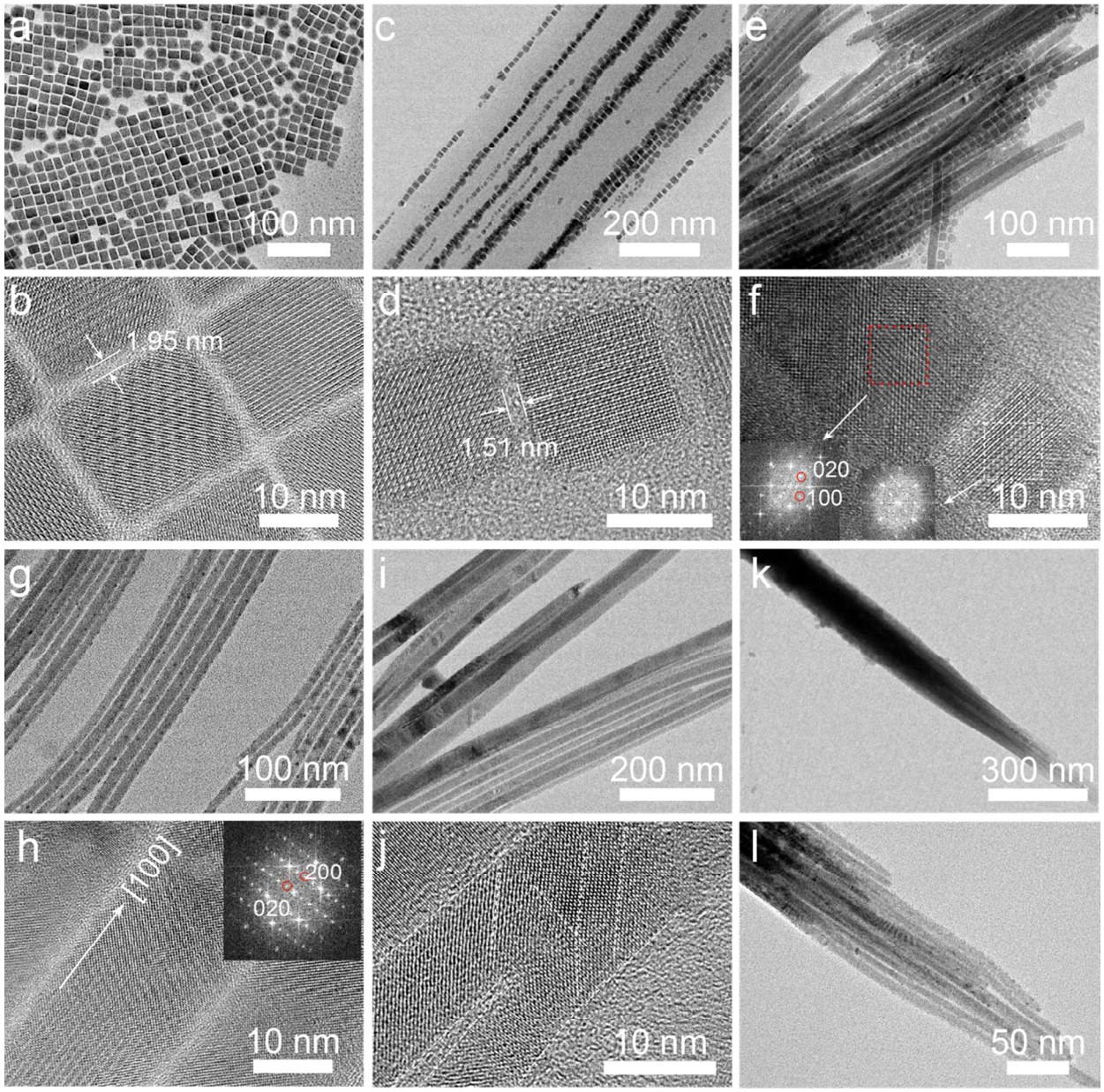

Figure 4. Low- and high-magnification TEM images displaying the time-dependent self-assembly of $CsPbI_3$ nanocubes into nanowires. (a, b) Original $CsPbI_3$ nanocubes. (c-f) Self-assembly of $CsPbI_3$ nanocubes at 1 min (c, d) and 5 min (e, f) after the addition of ethanol, respectively. The insets in f are the corresponding Fourier-transform diffractograms on the marked region. The red square region shows the evolved orthorhombic structure while the white square keeps distorted cubic structure. (g-l) Self-assembled $CsPbI_3$ nanowires in different diameters collected at 10 min (g, h), 20min (i, j), and 30 min (k, l) after the addition of ethanol, respectively. The insets in h is the corresponding Fourier-transform diffractogram.

more nanocubes to fuse into its end. The more nanocubes fuse into nanorod/nanowire the larger the dipole force is. Over time, the linearly self-assembled nanocubes evolves into single-crystalline nanowires in a width same as the nanocube, i.e. ~15 nm. The length of nanowires can reach over 5 μm (Figure S6), meaning over 300 nanocubes can self-assemble and fuse together in the same direction. Distinct from other oriented attachment and self-assembly in inorganic systems, the self-assembly and fusion of $CsPbI_3$ nanocubes take place very fast, probably due to the concomitant energy-favorable phase transition. It is believed that the phase transition process accompanies with lattice match and atomic reconstruction, resulting in the nanowires with nearly perfectly smooth surfaces although the building blocks (nanocubes) are not in perfectly cubic shape. After 10 min, all nanocubes evolve into $CsPbI_3$ nanowires with a uniform width corresponding to the size of single nanocube (Figure 4g). HRTEM image and diffraction pattern (Figure 4h) evidence that the nanowires are in orthorhombic phase and oriented in [100]

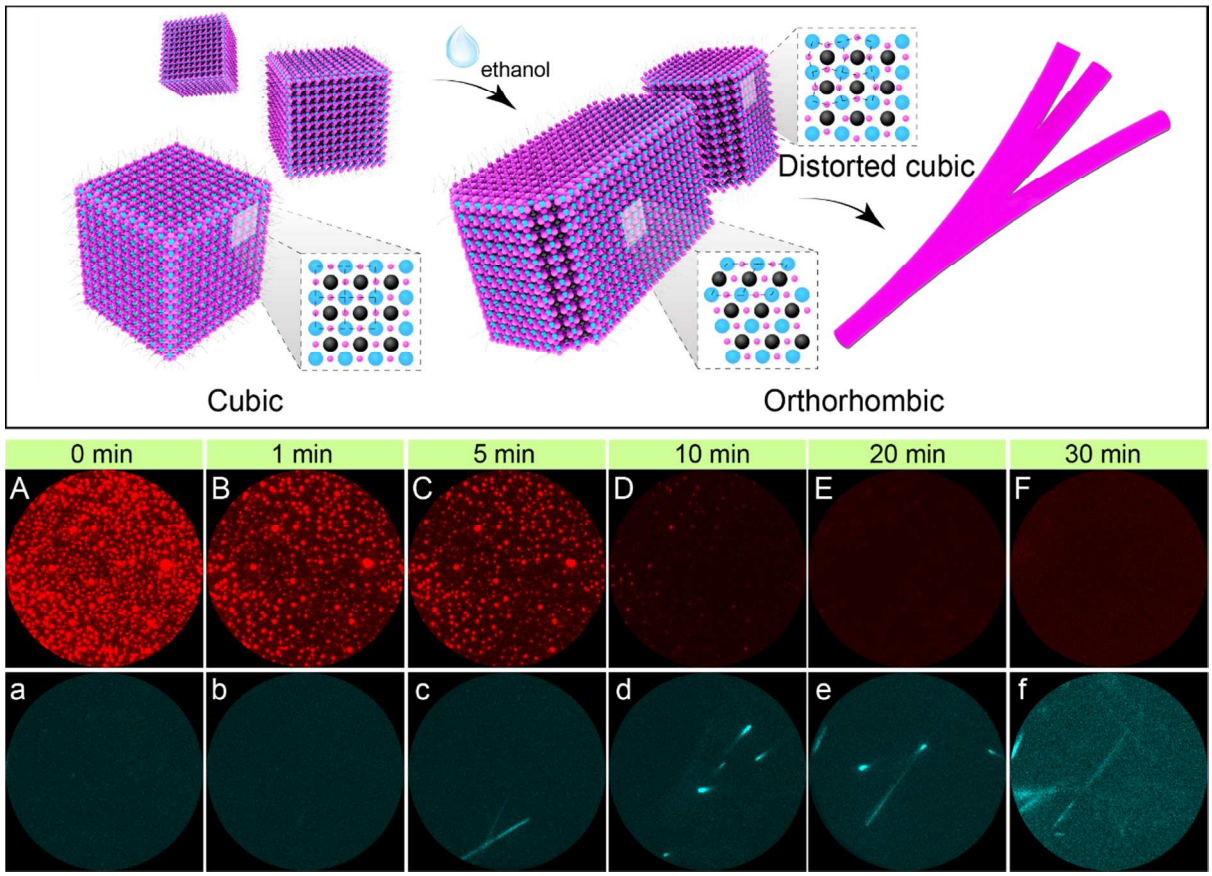

Figure 5. Schematic diagram (top image) and TIRFM micrographs of self-assembly process of CsPbI3 nanocubes into nanowires. TIRFM micrographs of (A-F) and (a-f) are captured through a D679/41 and D460/60 band-pass filter, respectively.

direction, which agrees with the calculated growth direction with lowest surface energy and double-chain nature of orthorhombic $CsPbI_3$ (Table S3).

Along with the evolution of $CsPbI_3$ nanocubes into nanowires with a large aspect ratio, it was found that when nanowires attached together side-by-side they could also fused into a thicker single-crystalline nanowire by lattice matching (Figure 4i). HRTEM image in Figure 4j shows a clear lattice matching process of two nanowires merging into one single-crystalline nanowire. A couple of initial nanowires can merge into thicker ones, which can further merge with other nanowires, leading to even thicker ones (Figure 4i). Through this hierarchical self-assembly and fusion process, the width of final nanowires can reach up to hundreds of nanometers building from a bunch of nanowires as shown in Figure 4k. While the zoom-in view TEM image clearly shows that its tail is still composed of a bunch of initial nanowires (in a width of nanocube size) (Figure 4l). This result further supports the proposed mechanism that the thick single-crystalline wire is formed by the oriented attachment and lattice fusion of thinner nanowires. The hierarchical self-assembly process of $CsPbI_3$ nanocubes into nanowires is schematically illustrated in the top of Figure 5. If the concentration of nanocubes is high, the self-assembly of nanocubes into nanowire and the secondary self-assembly of nanowires into thicker ones would take place simultaneously. The pre-formed nanowire parts have a chance to attach and merge with others while each nanowire can still attract nanocubes and keep growing. Therefore, it is usually seen that the final product contains broom-like nanowire bundles with merged end or middle part as well as unmerged nanowire end, as shown in Figure S6. It should be noted that the nanowire thickness and morphology in the final product can be controlled to some extent by adjusting the concentration of nanocubes in the solution, polar solvent amount, and assembling time. The less amount of nanocubes, polar solvent, or short time will deliver thinner final nanowires and less nanowire bundles.

It should be noted here that during the lattice distortion and self-assembly the polar solvent molecules did not go into the lattice $CsPbI_3$. We carefully checked the XRD patterns of orthorhombic $CsPbI_3$ nanowires after the self-assembly. As shown in Figure S7 There are no shifts of diffraction peaks compared with the standard reference (JCPDS No. 74-1970). The lattice fringes in HRTEM images (Figure 4h and Figure S8) also exactly match with the interplanar distances of the reference. Therefore, the polar solvent should induce the lattice distortion and initiate the self-assembly through the surface interaction instead of integrating into the lattice.

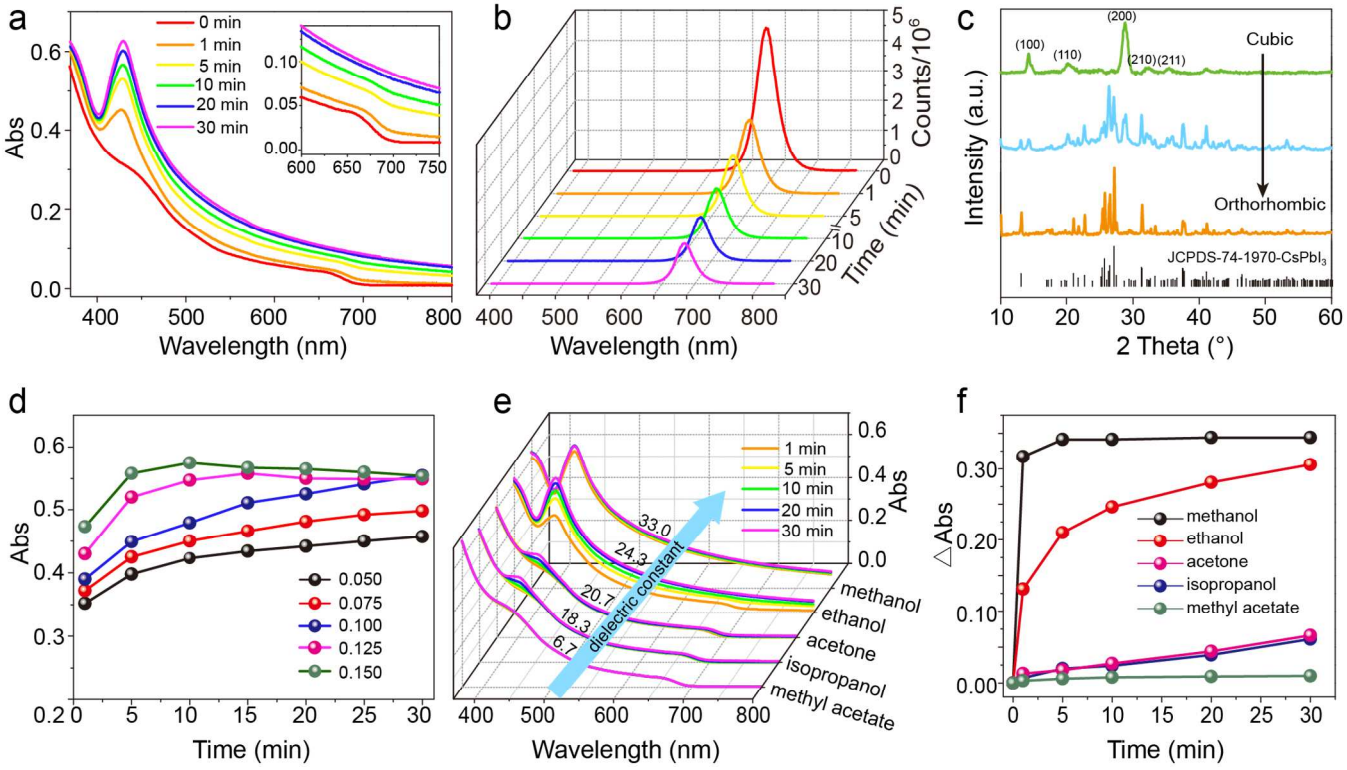

Figure 6. Time-dependent UV-vis absorption (a) and PL (b) spectra of $CsPbI_3$ at the different time after addition of 0.1 mL ethanol. The inset is the zoom-in view of Figure 6a in 600-750 nm. (c) XRD patterns of the products during ethanol-induced self-assembly. (d) Time-dependent absorbance (at about 430 nm) for different amounts of ethanol. (e-f) Time-dependent UV-vis absorption spectra (e) and the absorbance change (f) for polar solvents with different dielectric constants. 0.1 mL solvents are added.

3.5 In-situ monitoring hierarchal self-assembly of $CsPbI_3$ nanocubes. The polar molecule induced self-assembly and phase transition process of cubic $CsPbI_3$ nanocubes into orthorhombic nanowires were further monitored by fluorescence evolution. Fluorescence spectra (PL) indicate that pristine nanocubes show a very strong red emission at 690 nm, which is typical for cubic $CsPbI_3$, while assembled nanowires presents much weak blue emission centered at 445 nm corresponding to orthorhombic $CsPbI_3$ (Figure S9). A total internal reflection fluorescence microscope (TIRFM) with a resolution of single-molecule imaging was used to in-situ image the fluorescence evolution during the self-assembly process on a basis of the different emission from nanocubes and nanowires. Luminescence is divided to red and blue channel through D679/41 and D460/60 band-pass filter. For the red channel, the fluorescence was attenuated by OD4 dimmer to get clear images in view of too strong emission from cubic $CsPbI_3$. As shown in Figure 5A-F and Movie S1, the gradual fading of red fluorescence indicates the cubic $CsPbI_3$ disappears bit by bit over time. After 30 min, almost no red emission was observed in the red channel. Concomitantly, nanowire emission shows up and progressively increases in the blue channel (Figure 5a-f), indicating the formation of orthorhombic nanowires accompanying with the dissipation of nanocubes.

The kinetics of polar molecule induced self-assembly was investigated by UV-vis and PL spectroscopy. The optical photos show that the solution color gradually changes from red for initial $CsPbI_3$ nanocubes solution to yellow for self-assembled $CsPbI_3$ nanowire solution (Figure S10) in 30 min after the addition of 0.1 mL ethanol into 2 mL hexane containing ~1 mmol/mL $CsPbI_3$ nanocubes. In UV-vis spectra (Figure 6a), the absorption edges at ~700 nm from the cubic $CsPbI_3$ gradually fade away and distinct absorption peaks rise up at 430 nm, which can be assigned to the first absorption band of orthorhombic nanowires. Meanwhile, the optical photos taken under UV light show the solution color changes from red to blue. The photoluminescence (PL) spectra indicate that PL emission intensity at 690 nm gradually decrease, suggesting the self-assembly (Figure 6b). X-ray diffraction patterns were also recorded during the self-assembly process to reveal the phase transition process. As shown in Figure 6c, the diffraction peaks from orthorhombic $CsPbI_3$ clearly show up 30 min after the addition of ethanol and the peaks from cubic phase decrease. After 1 h, all diffractions can be indexed to orthorhombic $CsPbI_3$ and no cubic phase is detected, suggesting the completion of phase transition.

Furthermore, it was found that the kinetics of self-assembly is closely dependent on the amount and the dielectric constant of polar solvent. The absorptions at 430 nm are plotted as a function of time under the different adding amounts of ethanol. According to Figure 6d,

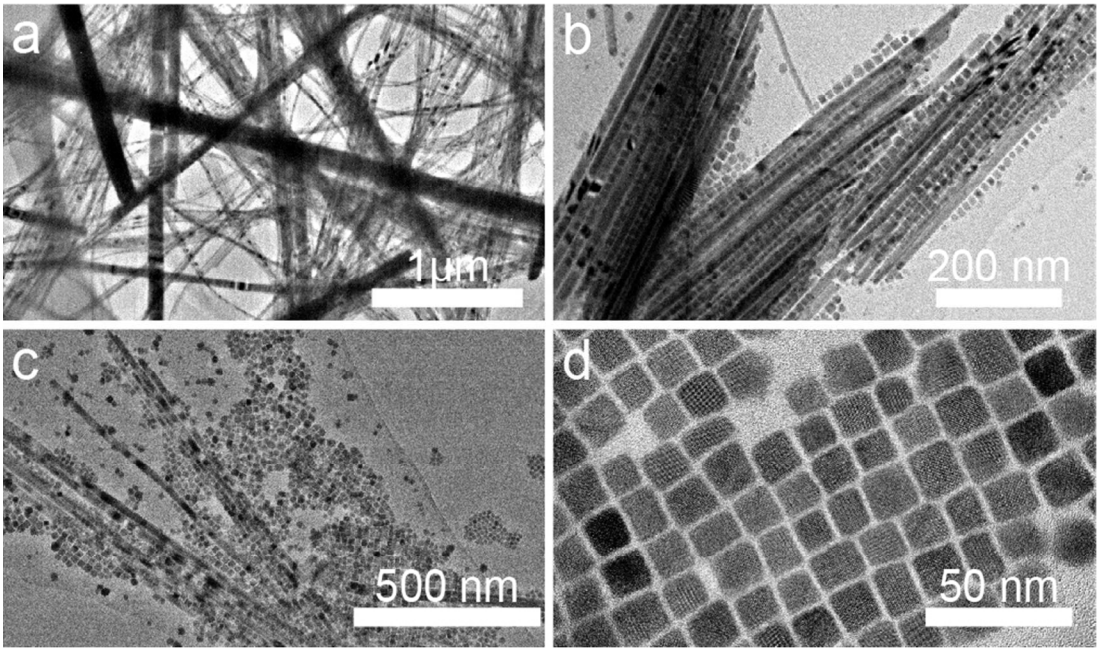

Figure 7. TEM images taken at 5 min after adding 0.1 mL of methanol (a), ethanol (b), isopropanol (c) and methyl acetate (d) into 1 mmol/mL CsPbI3 solution, respectively.

increasing ethanol addition can accelerate the self-assembly process. For example, 5 min after addition of 0.150 mL ethanol the absorption intensity reaches 95 % of maximum, similar to that 30 min after addition of 0.100 mL ethanol. While the absorption after 20 min in the case of 0.050 mL ethanol only reach 85 % of maximum, similar to that 1 min after addition of 0.125 mL ethanol.

The dielectric constant (ε) is a measure of solvent polarity. Higher dielectric constant means higher polarity and greater ability to induce the lattice distortion of $CsPbI_3$ nanocubes. The UV-vis spectra in Figure 6e clearly show the different kinetics of self-assembly in solvents with different dielectric constants. The solvent with higher dielectric constant can induce the self-assembly and phase transition much faster. For example, methanol (ε = 33.0) can induce the production of nanowires in 1 min. While the absorbance change in the case of isopropanol (ε = 18.3) and acetone (ε = 20.7) takes place much slower (Figure 6f). Moreover, methyl acetate was used to replace amine ligands on $CsPbI_3$ nanocubes while basically keeping their cubic phase, achieving $CsPbI_3$ quantum dot-based solar cells with a high efficiency of 10.77 %.[21] It can be seen in Figure 6e-f that methyl acetate (ε = 6.7) barely cause the change of absorption, rationalizing its application in the fabrication of high-efficiency $CsPbI_3$ solar cells. As a direct demonstration of the influence of solvent polarity on the self-assembly, TEM images were taken 5 min after adding different solvents (0.1 mL). As shown in Figure 7, the sample with methanol shows plenty of nanowires in several micrometer long and some nanowires are much thicker due to side-by-side self-assembly of primary nanowires (Figure 7a). The sample with ethanol (ε = 24.3) shows nanowires in a length of hundreds of nanometer and a width similar to nanocube size (Figure 7b). While the sample with isopropanol (ε = 18.3) is composed of plenty of nanocubes with a few nanowires (Figure 7c). For the methyl acetate (ε = 6.7), the sample does not exhibit detectable change from the pristine nanocubes and still consists of nanocubes (Figure 7d). No assembled nanowire or even larger nanocrystals are observed. These TEM results are well consistent with the above analyses.

Additionally, we are aware that the dielectric constants of the liquid solvents we used here increases as their molecular size decreases, but it does not mean the molecular size is the measure of the interaction between solvent and cubic $CsPbI_3$ nanocubes. To demonstrate this point, a control experiment was carried out. As mentioned, the as-synthesized cubic-phase $CsPbI_3$ nanocrystals are very stable in hexane due to its non-polarity. However, when we use 1-octyl alcohol with a larger size and dielectric constant as well than hexane (10.914 Å vs. 8.095Å for size and 3.4 vs. 2.0 for dielectric constant) as the polar solvent to disperse cubic $CsPbI_3$ nanocrystals, the phase transition and self-assembly will take place in tens of minutes, as implied by the optical image in Figure S11. Since the polar solvent acts through surface interaction instead of going into the lattice, it is more reasonable that the solvent polarity matters its interaction with $CsPbI_3$ rather than its size.

4. Conclusion

In conclusion, we found for the first time here that polar molecules can induce the lattice distortion of ligand-stabilized cubic $CsPbI_3$, triggering the dipole moments. The theoretical analyses indicate that the attachment of polar molecules causes the move of metal ions in perovskite and the distortion of PbI_6 octahedra, which is directly visualized and evidenced by atomic resolution transmission electron microscopic observation. The induced dipole moment drives the self-assembly of $CsPbI_3$ nanocubes into single-crystalline nanowires under OA mechanism, accompanying with the phase transition from cubic into orthorhombic phase. The formed $CsPbI_3$ nanowires can further hierarchically side-by-side self-assembled into much thicker nanowires up to submicrometer in width. Importantly, the systematic

investigation on the kinetics of self-assembly reveals that the more amount or the stronger polarity of polar solvent can induce the more rapid self-assembly and phase transition. These results not only provide the new insight into the destabilization of cubic $CsPbI_3$ nanocrystals, but also guide to explore strategies for the synthesis and store of cubic $CsPbI_3$ materials by properly selecting solvents, leading to the potential for their practical applications in photovoltaics and optoelectronics.

ASSOCIATED CONTENT

Supporting Information.

FTIR spectra, PL spectra, additional XRD patterns and TEM images, time-dependent inter-distances statistics during self-assembly process, and supplementary theoretical calculation analyses are provided as Supporting Information which are available free of charge via the Internet at http://pubs.acs.org.

AUTHOR INFORMATION

Corresponding Author

*hujs@iccas.ac.cn

*wanlijun@iccas.ac.cn

Author Contributions

▽These authors contributed equally.

Notes

The authors declare no competing financial interest.

ACKNOWLEDGMENT

This work was supported by the National Key Project on Basic Research (2015CB932302), National Natural Science Foundation of China (21573249, and 91645123) and the Strategic Priority Research Program of the Chinese Academy of Sciences (XDB12020100).

REFERENCES

(1) Yang, W. S.; Park, B. W.; Jung, E. H.; Jeon, N. J.; Kim, Y. C.; Lee, D. U.; Shin, S. S.; Seo, J.; Kim, E. K.; Noh, J. H.; Seok, S. I. *Science* **2017**, *356*, 1376.

(2) You, J.; Meng, L.; Song, T.-B.; Guo, T. F.; Yang, Y.; Chang, W.-H.; Hong, Z.; Chen, H.; Zhou, H.; Chen, Q.; Liu, Y.; De Marco, N.; Yang, Y. *Nat. Nanotechnol.* **2015**, *11*, 75.

(3) Saliba, M.; Matsui, T.; Seo, J. Y.; Domanski, K.; Correa-Baena, J. P.; Nazeeruddin, M. K.; Zakeeruddin, S. M.; Tress, W.; Abate, A.; Hagfeldt, A.; Gratzel, M. *Energy Environ. Sci.* **2016**, *9*, 1989.

(4) Chen, W.; Wu, Y.; Yue, Y.; Liu, J.; Zhang, W.; Yang, X.; Chen, H.; Bi, E.; Ashraful, I.; Grätzel, M.; Han, L. *Science* **2015**, *350*, 944.

(5) Yi, C.; Luo, J.; Meloni, S.; Boziki, A.; Ashari-Astani, N.; Gratzel, C.; Zakeeruddin, S. M.; Rothlisberger, U.; Gratzel, M. *Energy Environ. Sci.* **2016**, *9*, 656.

(6) Park, N. G.; Grätzel, M.; Miyasaka, T.; Zhu, K.; Emery, K. *Nat. Energy* **2016**, *1*, 16152.

(7) Filip, M. R.; Eperon, G. E.; Snaith, H. J.; Giustino, F. *Nat. Commun.* **2014**, *5*, 5757.

(8) Song, J.; Li, J.; Li, X.;. Xu, L.; Dong, Y., Zeng, H. *Adv. Mater.* **2015**, *27*, 7162.

(9) Huang, H.; Polavarapu, L.; Sichert, J. A.; Susha, A. S.; Urban, A. S.; Rogach, A. L. *NPG Asia Mater.* **2016**, *8*, e328.

(10) Li, X.; Cao, F.; Yu, D.;Chen, J.; Sun, Z.; Shen, Y.; Zhu, Y.; Wang, L.; Wei, Y.; Wu, Y.; Zeng, H. *Small* **2017**, *13*, 1603996.

(11) Cho, H.; Jeong, S. H.; Park, M. H.; Kim, Y. H.; Wolf, C.; Lee, C. L.; Heo, J. H.; Sadhanala, A.; Myoung, N.; Yoo, S.; Im, S. H.; Friend, R. H.; Lee, T. W. *Science* **2015**, *350*, 1222.

(12) Zhou, Q.; Bai, Z.; Lu, W. G.; Wang, Y.; Zou, B.; Zhong, H. *Adv. Mater.* **2016**, *28*, 9163.

(13) Chang, S.; Bai, Z.; Zhong, H. *Adv. Optical. Mater.* **2018**, 6, 1800380.

(14) Stoumpos, C. C.; Malliakas, C. D.; Peters, J. A.; Liu, Z.; Sebastian, M.; Im, J.; Chasapis, T. C.; Wibowo, A. C.; Chung, D. Y.; Freeman, A. J.; Wessels, B. W.; Kanatzidis, M. G. *Cryst. Growth Des.* **2013**, *13*, 2722.

(15) Kulbak, M.; Cahen, D.; Hodes, G. *J. Phys. Chem. Lett.* **2015**, *6*, 2452.

(16) Hoffman, J. B.; Schleper, A. L.; Kamat, P. V. *J. Am. Chem. Soc.* **2016**, *138*, 8603.

(17) Lee, J. W.; Kim, D. H.; Kim, H. S.; Seo, S. W.; Cho, S. M.; Park, N. G. *Adv. Energy Mater.* **2015**, *5*, 1501310.

(18) Liang, J.; Wang, C.; Wang, Y.; Xu, Z.; Lu, Z.; Ma, Y.; Zhu, H.; Hu, Y.; Xiao, C.; Yi, X.; Zhu, G.; Lv, H.; Ma, L.; Chen, T.; Tie, Z.; Jin, Z.; Liu, J. *J. Am. Chem. Soc.* **2016**, *138*, 15829.

(19) Chen, C. Y.; Lin, H. Y.; Chiang, K. M.; Tsai, W. L.; Huang, Y. C.; Tsao, C. S.; Lin, H. W. *Adv. Mater.* **2017**, *29*, 1605290.

(20) Protesescu, L.; Yakunin, S.; Bodnarchuk, M. I.; Krieg, F.; Caputo, R.; Hendon, C. H.; Yang, R. X.; Walsh, A.; Kovalenko, M. V. *Nano Lett.* **2015**, *15*, 3692.

(21) Swarnkar, A.; Marshall, A. R.; Sanehira, E. M.; Chernomordik, B. D.; Moore, D. T.; Christians, J. A.; Chakrabarti, T.; Luther, J. M. *Science* **2016**, *354*, 92.

(22) Sanehira, E. M.; Marshall, A. R.; Christians, J. A.; Harvey, S. P.; Ciesielski, P. N.; Wheeler, L. M.; Schulz, P.; Lin, L. Y.; Beard, M. C.; Luther, J. M. *Sci. Adv.* **2017**, 3, eaao4204.

(23) Zhang, T.; Dar, M. I.; Li, G.; Xu, F.; Guo, N.; Grätzel, M.; Zhao, Y. *Sci. Adv.* **2017**, 3, e1700841.

(24) Liu, C.; Li, W.; Zhang, C.; Ma, Y.; Fan, J.; Mai, Y. *J. Am. Chem. Soc.* **2018**, *140*, 3825.

(25) Lin, J.; Lai, M.; Dou, L.; Kley, C. S.; Chen, H.; Peng, F.; Sun, J.; Lu, D.; Hawks, S. A.; Xie, C.; Cui, F.; Alivisatos, A. P.; Limmer, D. T.; Yang, P. *Nat. Mater.* **2018**, *17*, 261.

(26) Sutton, R. J.; Eperon, G. E.; Miranda, L.; Parrott, E. S.; Kamino, B. A.; Patel, J. B.; Hörantner, M. T.; Johnston, M. B.; Haghighirad, A. A.; Moore, D. T.; Snaith, H. J. *Adv. Energy Mater.* **2016**, 6, 1502458.

(27) Sun, S.; Yuan, D.; Xu, Y.; Wang, A.; Deng, Z. *ACS Nano* **2016**, *10*, 3648.

(28) Pan, A.; He, B.; Fan, X.; Liu, Z.; Urban, J. J.; Alivisatos, A. P.; He, L.; Liu, Y. *ACS Nano* **2016**, *10*, 7943.

(29) Udayabhaskararao, T.; Houben, L.; Cohen, H.; Menahem, M.; Pinkas, I.; Avram, L.; Wolf, T.; Teitelboim, A.; Leskes, M.; Yaffe, O.; Oron, D.; Kazes, M. *Chem. Mater.* **2018**, *30*, 84.

(30) Liu, Z.; Bekenstein, Y.; Ye, X.; Nguyen, S. C.; Swabeck, J.; Zhang, D.; Lee, S. T.; Yang, P.; Ma, W.; Alivisatos, A. P. *J. Am. Chem. Soc.* **2017**, *139*, 5309.

(31) Bekenstein, Y.; Koscher, B. A.; Eaton, S. W.; Yang, P.; Alivisatos, A. P. *J. Am. Chem. Soc.* **2015**, *137*, 16008.

(32) Akkerman, Q. A.; Motti, S. G.; Srimath Kandada, A. R.; Mosconi, E.; D'Innocenzo, V.; Bertoni, G.; Marras, S.; Kamino, B. A.; Miranda, L.; De Angelis, F.; Petrozza, A.; Prato, M.; Manna, L. *J. Am. Chem. Soc.* **2016**, *138*, 1010.

(33) Bekenstein, Y.; Koscher, B. A.; Eaton, S. W.; Yang, P.; Alivisatos, A. P. *J. Am. Chem. Soc.* **2015**, *137*, 16008.

(34) Shanbhag, S.; Kotov, N. A. *J. Phys. Chem. B* **2006**, *110*, 12211.

(35) Tang, Z.; Kotov, N. A.; Giersig, M. *Science* **2002**, *297*, 237.

(36) Cho, K. S.; Talapin, D. V.; Gaschler, W.; Murray, C. B. *J. Am. Chem. Soc.* **2005**, *127*, 7140.

(37) Sinyagin, A. Y.; Belov, A.; Tang, Z.; Kotov, N. A. *J. Phys. Chem. B* **2006**, *110*, 7500.

(38) Boettger, J. C. *Phys. Rev. B* **1994**, *49*, 16798.

(39) Vincenzo, F.; Methfessel, M. *J. Phys.: Condens. Matter* **1996**, *8*, 6525.

(40) Bruno, M.; Prencipe, M. *CrystEngComm* **2013**, *15*, 6736.

(41) Jia, W.; Fu, J.; Cao, Z.; Wang, L.; Chi, X.; Gao, W.; Wang, L. W. *J. Comput. Phys.* **2013**, *251*, 102.

(42) Jia, W.; Cao, Z.; Wang, L.; Fu, J.; Chi, X.; Gao, W.; Wang, L. W. *Comput. Phys. Commun.* **2013**, *184*, 9.

(43) Frisch, M. J.; Trucks, G. W.; Schlegel, H. B.; Scuseria, G. E.; Robb, M. A.; Cheeseman, J. R.; Scalmani, G.; Barone, V.; Mennucci, B.; Petersson, G. A.; Nakatsuji, H.; Caricato, M.; Li, X.; Hratchian, H. P.; Izmaylov, A. F.; Bloino, J.; Zheng, G.; Sonnenberg, J. L.; Hada, M.; Ehara, M.; Toyota, K.; Fukuda, R.; Hasegawa, J.; Ishida, M.; Nakajima, T.; Honda, Y.; Kitao, O.; Nakai, H.; Vreven, T.; Montgomery, J. A., Jr.; Peralta, J. E.; Ogliaro, F.; Bearpark, M.; Heyd, J. J.; Brothers, E.; Kudin, K. N.; Staroverov, V. N.; Kobayashi, R.; Normand, J.; Raghavachari, K.; Rendell, A.; Burant, J. C.; Iyengar, S. S.; Tomasi, J.; Cossi, M.; Rega, N.; Millam, J. M.; Klene, M.; Knox, J. E.; Cross, J. B.; Bakken, V.; Adamo, C.; Jaramillo, J.; Gomperts, R.; Stratmann, R. E.; Yazyev, O.; Austin, A. J.; Cammi, R.; Pomelli, C.; Ochterski, J. W.; Martin, R. L.; Morokuma, K.; Zakrzewski, V. G.; Voth, G. A.; Salvador, P.; Dannenberg, J. J.; Dapprich, S.; Daniels, A. D.; Farkas, Ö .; Foresman, J. B.; Ortiz, J. V.; Cioslowski, J.; Fox, D. J. Gaussian 09, revision D.01; Gaussian, Inc.: Wallingford, CT, 2009.

(44) Frost, J. M.; Butler, K. T.; Walsh, A. *APL Mater.* **2014**, *2*, 081506.

(45) Burrows, N. D.; Vartanian, A. M.; Abadeer, N. S.; Grzincic, E. M.; Jacob, L. M.; Lin, W.; Li, J.; Dennison, J. M.; Hinman, J. G.; Murphy, C. J. *J. Phys. Chem. Lett.* **2016**, *7*, 632.

(46) De Roo, J.; Ibáñez, M.; Geiregat, P.; Nedelcu, G.; Walravens, W.; Maes, J.; Martins, J. C.; Van Driessche, I.; Kovalenko, M. V.; Hens, Z. *ACS Nano* **2016**, *10*, 2071.

(47) Min, Y.; Akbulut, M.; Kristiansen, K.; Golan, Y.; Israelachvili, J. *Nat. Mater.* **2008**, *7*, 527.

(48) Whitesides, G.; Mathias, J.; Seto, C. *Science* **1991**, *254*, 1312.

(49) Boal, A. K.; Ilhan, F.; DeRouchey, J. E.; Thurn-Albrecht, T.; Russell, T. P.; Rotello, V. M. *Nature* **2000**, *404*, 746.

(50) Carey, G. H.; Abdelhady, A. L.; Ning, Z.; Thon, S. M.; Bakr, O. M.; Sargent, E. H. *Chem. Rev.* **2015**, *115*, 12732.

(51) Penn, R. L.; Banfield, J. F. *Science* **1998**, *281*, 969.

TOC

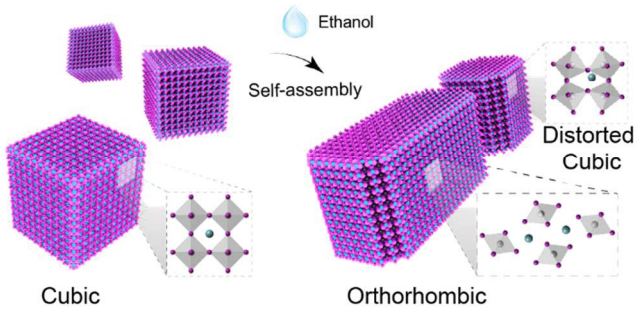
Ethanol
Self-assembly
Distorted
Cubic
Cubic
Orthorhombic